Simultaneous high-pressure and high-temperature volume measurements of ice VII and its thermal equation of state

Simultaneous high-pressure and high-temperature volume measurements of ice VII and its thermal equation of state

Emiko Sugimura,[1,*] Tetsuya Komabayashi,[1] Kei Hirose,[1,2] Nagayoshi Sata,[2] Yasuo Ohishi,[3] and Leonid S. Dubrovinsky[4]
[1]*Department of Earth and Planetary Sciences, Tokyo Institute of Technology, 2-12-1 Ookayama, Meguro, Tokyo 152-8551, Japan*
[2]*Institute for Research on Earth Evolution, Japan Agency for Marine-Earth Science and Technology, 2-15 Natsushima-cho, Yokosuka, Kanagawa 237-0061, Japan*
[3]*Japan Synchrotron Radiation Research Institute, 1-1-1 Kouto, Sayo, Hyogo 679-5198, Japan*
[4]*Bayerisches Geoinstitut, Universität Bayreuth, Bayreuth 95440, Germany*
(Received 5 July 2010; revised manuscript received 30 August 2010; published 5 October 2010)

We conducted simultaneous high-pressure (P) and high-temperature (T) unit-cell volume (V) measurements of H_2O ice VII in an externally heated diamond anvil cell using *in situ* synchrotron x-ray diffraction technique with an angle-dispersive system. Isothermal unit-cell volume of ice VII was collected at $P=33-50$ GPa with $T=873$ K. Nonisothermal experiments at $T=430-740$ K and $P=19-37$ GPa were also conducted to further constrain P-V-T properties of ice VII. Using the existing 300 K compression data for an equation of state (EoS) at the reference temperature, a thermal EoS of ice VII was constructed from the collected high-P-T data. The melting temperature of ice VII was computed up to $P=40$ GPa by thermodynamic calculations with the newly constructed EoS of ice VII. The resulting melting temperatures are higher than that of previous calculations since the new EoS gives a smaller molar volume of ice VII. In contrast, the calculated melting curves are consistent with recent experimental estimates.

DOI: 10.1103/PhysRevB.82.134103 PACS number(s): 64.30.−t, 62.50.−p, 61.05.cp, 64.70.dj

I. INTRODUCTION

Physical properties of H_2O at high-pressure (P) and high-temperature (T) have been under deep interest in condensed matter physics and chemistry, and planetary sciences. Equation of state (EoS) of solid H_2O plays an important role in understanding hydrogen bond behavior under extreme P-T conditions. Melting curve of H_2O is the primary information for modeling the deep interiors of icy planets such as Neptune and Uranus,[1] and for discussing the possible existence of H_2O solid phase in Earth's deep mantle that may have been delivered by cold subducting slabs.[2]

Ice VII is one of the 15 known solid phases of H_2O, and it appears above $P=2.2$ GP at room temperature along compression after the liquid to ice VI transformation at $P=0.9$ GPa. Ice VII takes a body-centered-cubic (bcc) oxygen sublattice and this simple structure is preserved to a very high pressure of 170 GPa.[3] The experimental evidence for the pressure-induced phase transition of ice VII, preserving the *bcc* oxygen sublattice, was found based on indirect methods such as spectroscopic[4–6] and x-ray diffraction (XRD) studies,[3,7] in which the hydrogen bond symmetrization was suggested to occur at pressure ranging from 40 to 66 GPa at $T=300$ K. Theoretical studies demonstrated that the hydrogen bond symmetrization in ice involves a gradual transition through intermediate phases, dynamically disordered ice VII and dynamically disordered ice X.[8–10] The existence of dynamically disordered ice VII at $T=300$ K has also been repeatedly proposed by a number of experimental studies with infrared spectroscopy[11,12] and Raman spectroscopy[13] As mentioned above, all of those symmetrization-related phases preserve their bcc oxygen sublattice and no resolvable changes in P-V relation was observed at the transitions in numbers of XRD compression studies.[3,7,14,15]

However, a recent study by Sugimura *et al.*[16] demonstrated, from the *in situ* angle-dispersive XRD experiments, that ice changes its compressibility at $P=40$ and 60 GPa at room temperature, which correspond to a transition of ice VII to dynamically disordered ice VII, and the subsequent transformation to dynamically disordered ice X, respectively. They also operated theoretical calculations to confirm the anomalous volume reduction at pressures between 40 and 60 GPa, and proposed highly compressible behavior of dynamically disordered ice VII. This signified that even though bcc oxygen sublattice is preserved through the phase transitions which are related to the hydrogen-bond symmetrization, the EoS of ice must be evaluated separately for each phase. More importantly, their study suggested that in order to observe such a change in compressibility, the high-resolution XRD technique should be used. Recently a study by the quantum molecular-dynamics simulations[17] reproduced the 300 K data set of Sugimura *et al.*[16] and therefore confirmed the validity of their experimental observations.

In contrast to 300 K experiments, high-temperature experimental volumetric data for high-pressure ice are available only from two energy-dispersive XRD works. Fei *et al.*[18] collected the high-P-T volume data of ice at $P=6-20$ GPa and $T=300-650$ K, and the same group, Frank *et al.*[19] later extended the maximum pressure and temperature up to 60 GPa and 850 K. However, as mentioned above the use of the angle-dispersive XRD technique is required to observe a precise P-V relation of high-pressure ice. In addition, it is highly plausible that Frank *et al.*[19] included the data of dynamically disordered ice VII, which is significantly compressible compared with ice VII,[16] when constructing the P-V-T EoS of ice VII.

The aim of the present study is to construct the P-V-T EoS of ice VII from the volumetric data collected only from

its stability field. Moreover, the accurate volume data were obtained with the angle-dispersive XRD system as in Sugimura *et al.*[16] From the EoS, the melting curve of ice VII, which was previously calculated by Fei *et al.*[18] was revised. The resulting melting temperatures from the thermodynamic calculation was compared with experimentally determined melting curves based on various types of melting criteria such as electrical resistance, XRD, Raman spectroscopy, and optical observations.[18–26]

II. EXPERIMENTAL PROCEDURES

High-*P*-*T* conditions were generated in the Bayreuth-type externally heated diamond anvil cell (EHDAC).[27] For the heater, we used a cylindrical furnace where AlChrom-O wire (0.25 mm in diameter) was wound. Heating was performed by supplying electricity to the AlChrom-O wire from a dc power supply up to 110 V to reach 873 K. Temperature was measured by Alumel-Chromel (*K*-type) thermocouple, which was placed very close (about 2 mm) to the sample. Due to a large heater size compared with the sample, uniform heating across the sample chamber was achieved. The temperature fluctuation during the heating was very small (1 K) and the entire temperature uncertainty was less than 5 K.[27] The Bayreuth type EHDAC works at BL10XU, SPring-8.[28,29]

Deionized liquid H_2O was loaded into a hole drilled in a preindented rhenium gasket with fine powder of gold (Au) or platinum (Pt) used as an internal pressure calibrant. With flat 300 μm or beveled 200 μm culet diamond anvils, the sample was first compressed to several tens of gigapascals at room temperature. Temperature was increased by referring to the previously reported melting curves of H_2O ice,[18–26] although some measurements were conducted at temperatures above the several melting curves among those listed above. Details will be discussed later in Sec. IV.

Angle-dispersive XRD spectra were collected on an imaging plate (Rigaku-R-AXIS IV) at BL10XU of SPring-8. Monochromatic incident x-ray beam with a wavelength of 0.411–0.415 Å was collimated to 15–20 μm in diameter. The exposure time was 2 min. Two-dimensional (2D) XRD images were integrated as a function of 2θ angle using the fit-2D program[30] to obtain conventional one-dimensional diffraction patterns.

III. RESULTS

A. Experimental results

Total of five separate sets of high-*P*-*T* *in situ* XRD experiments were conducted. The *P*-*T* conditions for volume measurements are shown in Fig. 1. A typical XRD spectrum of the sample is illustrated in Fig. 2. The unit-cell volumes of ice were determined from (110) and (200) peaks of bcc structure for all the XRD data. The splitting of the diffraction peak of ice was not observed at any *P*-*T* condition, which may contradict a recent experimental study at $T=300$ K by Somayazulu *et al.*[15] This discrepancy will be discussed in Sec. IV.

The pressures were determined from the unit-cell volume of Au or Pt calculated from its (111), (200), and (220) diffraction lines. Sugimura *et al.*[16] used Pt as a pressure calibrant in 300 K experiments and their 300 K EoS was employed as a reference in this study. However, from a laser-heated DAC experiment, it is known that Pt may react with hydrogen to form a platinum hydride, PtH_X at $T=1350-1500$ K.[25,31] Hence, although the present experiments do not reach such high-*T* conditions, we employed Au which is expected to be less chemically reactive than Pt, as the main pressure calibrant and Pt as the secondary pressure calibrant throughout the experiments. In order to sustain the consistency between different calibrants, we used Fei *et al.*'s[32] self-consistent pressure scales for Au and Pt which should give the identical pressure. As shown in Fig. 2, we did not observe any XRD peaks that signify the formation of PtH_X at all experimental *P*-*T* conditions.

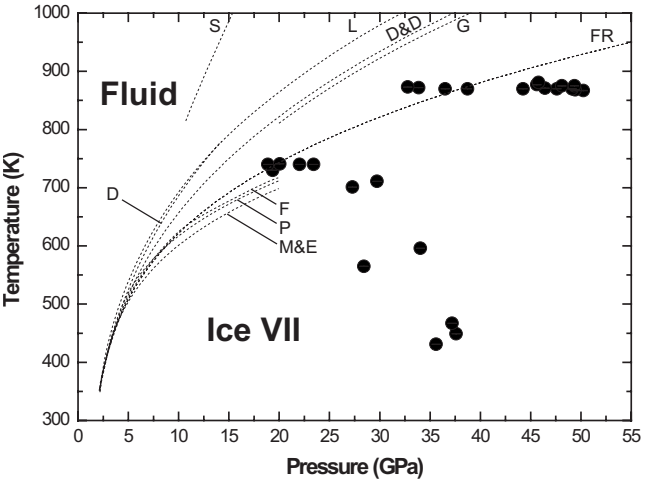

FIG. 1. Pressure-temperature conditions for unit-cell volume measurements of ice VII in the present experiments. Melting curves of ice VII proposed by previous studies are indicated by thin dotted lines. S, Schwager *et al.* (Ref. 25); L, Lin *et al.* (Ref. 24); D, Datchi *et al.* (Ref. 22); D&D, Dubrovinskaia and Dubrovinsky (Ref. 23); G, Goncharov *et al.* (Ref. 26); FR, Frank *et al.* (Ref. 19); F, Fei *et al.* (Ref. 18); P, Pistorius *et al.* (Ref. 20); and M&E, Mishima and Endo (Ref. 21).

The experimental conditions and the unit-cell volumes of H_2O ice are summarized in Table I. Isothermal *P*-*V* data at

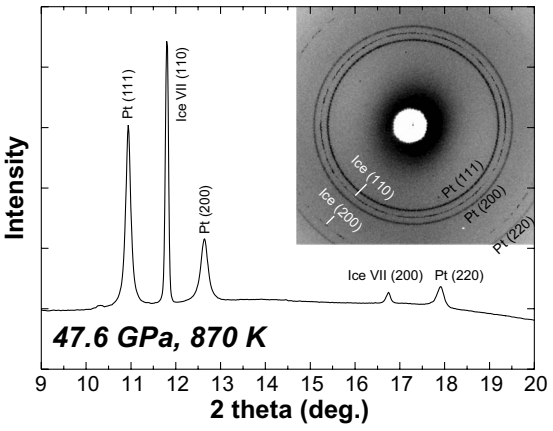

FIG. 2. X-ray diffraction pattern of *bcc* H_2O ice together with Pt at $P=47.6$ GPa, $T=870$ K. Inset, corresponding two dimensional x-ray diffraction pattern.

TABLE I. Experimental conditions and the volumes of H_2O ice VII.

Data	T (K)	P (GPa)	$V_{\text{Ice VII}}$ (cm^3/mol)	$a_{\text{Ice VII}}$ (Å)	a_{Au} (Å)	a_{Pt} (Å)	St
01-T16	431	35.60 ± 0.07	7.3378 ± 0.0002	2.8996 ± 0.0000	3.8939 ± 0.0003		−0.0003
02-T15	449	37.60 ± 0.30	7.2315 ± 0.0243	2.8855 ± 0.0032	3.8871 ± 0.0011		0.0024
03-T14	467	37.19 ± 0.07	7.2906 ± 0.0122	2.8933 ± 0.0016	3.8890 ± 0.0002		−0.0006
04-T15	565	28.42 ± 0.11	7.7935 ± 0.0288	2.9584 ± 0.0036	3.9264 ± 0.0004		0.0015
05-T16	596	34.03 ± 0.14	7.4923 ± 0.0042	2.9198 ± 0.0005	3.9046 ± 0.0005		0.0008
06-T15	701	27.29 ± 0.16	7.9492 ± 0.0173	2.9780 ± 0.0022	3.9356 ± 0.0007		0.0024
07-T15	711	29.72 ± 0.14	7.7995 ± 0.0130	2.9591 ± 0.0016	3.9255 ± 0.0006		0.0020
08-T16	730	19.36 ± 0.13	8.6262 ± 0.0091	3.0602 ± 0.0011	3.9744 ± 0.0007		0.0022
09-T16	740	18.88 ± 0.05	8.6910 ± 0.0068	3.0678 ± 0.0008	3.9773 ± 0.0003		0.0005
10-T16	740	22.04 ± 0.11	8.3774 ± 0.0196	3.0305 ± 0.0024	3.9614 ± 0.0006		0.0018
11-T16	740	23.43 ± 0.12	8.2695 ± 0.0107	3.0174 ± 0.0013	3.9546 ± 0.0006		0.0017
12-T16	741	20.06 ± 0.10	8.5665 ± 0.0026	3.0531 ± 0.0003	3.9712 ± 0.0005		0.0010
13-T09	867	50.25 ± 0.30	6.8932 ± 0.0150	2.8398 ± 0.0021		3.7667 ± 0.0008	−0.0003
14-T09	868	49.43 ± 0.12	6.9346 ± 0.0119	2.8455 ± 0.0016		3.7688 ± 0.0003	0.0001
15-T16	870	36.50 ± 0.17	7.4511 ± 0.0176	2.9144 ± 0.0023	3.9030 ± 0.0006		0.0021
16-T16	870	38.72 ± 0.26	7.3534 ± 0.0206	2.9016 ± 0.0027	3.8946 ± 0.0010		0.0032
17-T16	870	44.24 ± 0.26	7.1063 ± 0.0298	2.8687 ± 0.0040	3.8748 ± 0.0009		0.0032
18-T09	870	47.62 ± 0.32	6.9924 ± 0.0130	2.8533 ± 0.0018		3.7735 ± 0.0008	−0.0007
19-T09	870	49.12 ± 0.43	6.9467 ± 0.0138	2.8471 ± 0.0019		3.7696 ± 0.0011	−0.0020
20-T16	871	46.43 ± 0.27	7.0239 ± 0.0286	2.8576 ± 0.0039	3.8675 ± 0.0009		0.0031
21-T16	872	33.87 ± 0.16	7.5980 ± 0.0265	2.9334 ± 0.0034	3.9134 ± 0.0006		0.0022
22-T16	873	32.78 ± 0.24	7.6637 ± 0.0092	2.9419 ± 0.0012	3.9178 ± 0.0010		0.0027
23-T19	875	48.11 ± 0.19	6.9734 ± 0.0319	2.8508 ± 0.0043	3.8620 ± 0.0006		0.0019
24-T19	875	49.36 ± 0.40	6.9303 ± 0.0180	2.8449 ± 0.0025	3.8580 ± 0.0013		0.0045
25-T19	877	45.61 ± 0.11	7.0599 ± 0.0109	2.8625 ± 0.0015	3.8703 ± 0.0004		0.0012
26-T19	881	45.78 ± 0.11	7.0521 ± 0.0032	2.8614 ± 0.0004	3.8699 ± 0.0004		0.0006

T=867–880 K (~873 K) were collected at pressure from 33 to 50 GPa. In order to further constrain the P-V-T properties of ice VII, additional volume data were also collected at T=431–741 K and P=19–38 GPa. Figure 3 shows the collected volumes of H_2O ice plotted against the pressures, together with the isothermal compression data of ice VII at T=300 K.[16] The isothermal P-V data at T=873 K run almost parallel to the 300 K isotherm of ice VII, suggesting the data were collected well within the stability field of ice VII. Namely, an anomalous volume reduction, the plausible signature of the phase transition of ice VII to dynamically disordered ice VII, did not occur at the pressure range of the present experiments. Hence, it can be inferred that ice VII is stable at T=873 K at least to P=50 GPa.

In the high-pressure experiments using a DAC, the hydrostatic state of the sample must be somewhat evaluated, because it is a significant issue concerning the compression behavior of solid materials,[33,34] especially since pressure medium was not used in the present experiments. We followed the method proposed by Shim *et al.*[34] who used St value as an indicator of the magnitude of the uniaxial stress component in a cubic sample; S is the elastic anisotropy and t is the uniaxial stress component (see Shim *et al.*[34] for details). Here, St value of each experimental data was calculated from (111), (200), and (220) peaks of Au or Pt mixed with the sample. The estimated St for each data point is listed in Table I. In our P-V-T data set, the St value ranges from −0.0020 to

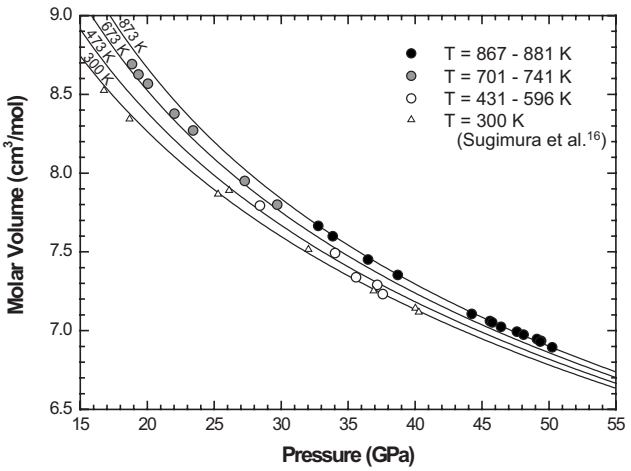

FIG. 3. Molar volumes of H_2O ice VII. Isotherms are calculated at T=300, 473, 673, and 873 K from EoS with parameters listed in Table II. The circles are the high-temperature data collected in this study and the triangles are the 300 K experimental data of ice VII from Sugimura *et al.* (Ref. 16).

TABLE II. Thermoelastic parameters of H_2O ice VII.

	V_0 (cm^3/mol)	K_0 (GPa)	K'	α_0 (10^{-5}/K)	δ_T
This study	14.52[a]	5.02	7.51	150 ± 19	5.1 ± 0.2
Fei *et al.*[b]	12.3 ± 0.2	23.9 ± 0.7	4.2 ± 0.5	6.0	
Frank *et al.*[c]	12.4 ± 0.1	21.1 ± 1.3	4.4 ± 0.1	4.8	

[a]From Loubeyre *et al.* (Ref. 3).
[b]Reference 18.
[c]Reference 19.

0.0045. If S is available, one can calculate the deviatoric stress from St. However, since S varies with pressure (e.g., Duffy *et al.*[35]) and its pressure dependence for Au and Pt is unknown, we cannot directly estimate the deviatoric stress in the sample. For reference, Shim *et al.*[36] reported the $|St|$ value of $CaSiO_3$ perovskite at $P=18-96$ GPa and $T=1238-2419$ K ranged from -0.005 to 0.005. In addition, Dubrovinsky *et al.*[37] reported that deviatoric stress in MgO is as small as 0.25 GPa at $T=850$ K. Therefore, the stress state in the present EHDAC was expected to be minimal.

B. *P-V-T* equation of state of ice VII

The *P-V-T* EoS of ice VII was constructed from the high-temperature data collected in this study. The existing EoS at $T=300$ K (Ref. 16) which was obtained by the same experimental technique as in this study was used as the reference temperature EoS. The molar volumes of ice VII at $T=300$ K are described with the Vinet EoS

$$P = 3K_0 x^{-2}(1-x)\exp\left[\frac{3}{2}(K'-1)(1-x)\right], \quad (1)$$

where $x=(V/V_0)^{1/3}$, and V_0, K_0, and K' are the molar volume, isothermal bulk modulus, and its pressure derivative, respectively, at ambient condition. Here, $V_0=14.52$ cm^3/mol, $K_0=5.02$ GPa, and $K'=7.51$ for ice VII from Sugimura *et al.*[16] are adopted.

In order to extend EoS to high temperatures, we express the thermal expansivity as a function of pressure in the framework of the Anderson-Grüneisen expression,[38] described as

$$(\alpha/\alpha_0) = (V/V_0)^{\delta_T}, \quad (2)$$

where α and α_0 are the thermal expansivity at a pressure of interest and ambient pressure, respectively. The parameter δ_T is so-called Anderson-Grüneisen parameter. A least-square fitting of our high-pressure and high-temperature data yielded $\alpha_0=150 \pm 19 \times 10^{-5}$/K and $\delta_T=5.1 \pm 0.2$. The obtained parameters are summarized in Table II. In Fig. 4, the calculated isotherms at every 100 K of ice VII up to $T=900$ K are illustrated together with collected high-temperature volume data, in terms of the difference from those of room temperature at corresponding pressure, $V(P,T)$-$V(P,300$ K). Figure 4 emphasizes that the experimental data are well reproduced by the *P-V-T* EoS with the obtained parameters.

C. Melting curve of ice VII

Melting of ice VII is defined by the equilibrium of the reaction of H_2O (ice VII)$=H_2O$ (fluid). On the equilibrium *P-T* conditions, the Gibbs free energy difference between the two phases is zero, namely,

$$\Delta G_{r(\text{IceVII-Water})} = 0 = \Delta H_r^{\mathrm{O}} + \int_{T_0}^{T} \Delta C_{P\ r}^{\mathrm{O}}\, dT - T\left(\Delta S_r^{\mathrm{O}} + \int_{T_0}^{T} \frac{\Delta C_{P\ r}^{\mathrm{O}}}{T} dT\right) + \int_{P_0}^{P} \Delta V_r\, dP \quad (3)$$

where ΔG_r is a Gibbs free energy change in the reaction, ΔH_r^{O}, ΔS_r^{O}, $\Delta C_{P\ r}^{\mathrm{O}}$, and ΔV_r are the changes in the reaction in enthalpy, entropy, heat capacity, and molar volume, respectively. The reference *P-T* condition is 1 bar and 300 K. The superscript O on each parameter denotes 1 bar. The ΔH_r^{O} and ΔS_r^{O} are calculated from the difference between each phase in the standard enthalpy of formation from the elements ($\Delta_f H^{\mathrm{O}}$) and standard entropy (S^{O}), both of which are at the reference *P-T* conditions. The Gibbs free energy of fluid H_2O at $P=1$ bar and T of interest is given by Robie *et al.*[39]

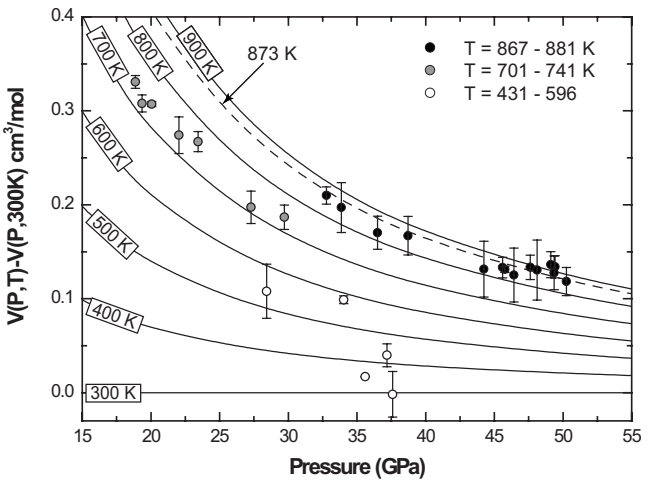

FIG. 4. Molar volumes of H_2O ice VII relative to the volumes at 300 K. Isotherms (solid lines) are calculated from the EoS in this study in every 100 K up to 900 K. The horizontal line represents the reference isotherm that is of 300 K (Ref. 16). The dashed line represents the calculated 873 K isotherm, which well reproduces the 873 K experimental data (closed circles).

TABLE III. Thermochemical parameters for melting temperature calculation.

			$C_P^o = a + bT + cT^{-2} + dT^2 + eT^{-0.5}$ (J/mol* K)				
	$\Delta_f H^o$ (kJ/mol)	S^o (J/mol* K)	a	b ($\times 10^{-3}$)	c ($\times 10^{5}$)	d ($\times 10^{-6}$)	e ($\times 10^{2}$)
Water[a]	−241.8	188.83	7.3680	27.468	−2.2316	−4.8117	3.6174
Ice VII[b]	−282.6	68	72.49	3.0240	−14.420		

[a]All data were taken from Robie *et al.* (Ref. 39).
[b]$\Delta_f H^o$ and S^o were determined in this study from thermodynamic calculation using EoS of water from Belonoshko and Saxena (Ref. 41). Coefficients for C_p^o were taken for from Fei *et al.* (Ref. 18).

Using their *P-V-T* EoS for ice VII, Fei *et al.*[18] obtained $\Delta_f H^O$, S^O, and C_P^O for ice VII by fitting previously published experimental data[20] up to $P=5$ GPa. From the determined parameters, they calculated the melting temperatures of ice VII at pressures from 5 to 20 GPa, which are fairly consistent with the result of their melting experiments.

We revisited the thermodynamic calculation of the melting of ice VII by replacing the *P-V-T* EoS for ice VII with that in this study. The present purpose is to evaluate the effect of *P-V-T* EoS for ice VII on the calculated melting temperature. For $\Delta_f H^O$, S^O, and C_P^O of fluid H_2O, we adopted the data in Robie *et al.*[39] same as in Fei *et al.*[18] The heat capacity for ice VII was also from Fei *et al.*[18] The specific values of each parameter are summarized in Table III. For the calculation of fluid fugacity, we used EoS proposed by Halbach and Chatterjee[40] and Belonoshko and Saxena[41] which were used in Fei *et al.*[18] In addition, we tested another EoS by Brodholt and Wood.[42] We derived $\Delta_f H^O$ and S^O for ice VII to reproduce the experimental data of melting temperature up to $P=5$ GPa.[20] Note that the set of $\Delta_f H^O$ and S^O was obtained for each of three calculations with different EoS of fluid H_2O. Figure 5 shows the calculated melting temperatures of ice VII. Comparison of the curves between this study and Fei *et al.*[18] shows that the melting temperature in this study is slightly lower at pressures below 13 GPa (with fluid EoS by Halbach and Chatterjee[40]) and 11 GPa (with fluid EoS by Belonoshko and Saxena[41]). However, beyond those pressures, our melting curve gives higher temperatures.

IV. DISCUSSIONS

A. *P-V-T* equation of state of ice VII

Newly determined *P-V-T* EoS of ice VII in this study is compared with that of previous studies[18,19] in Table II and Fig. 6. Our thermal expansivity at $P=1$ bar (α_0) is very large compared with that of the previous estimates[18,19] (Table II). This apparent discrepancy comes from the difference in the formulation of EoS at $T=300$ K. Since ice VII is not quenchable to $P=1$ bar, the 1 bar parameters of V_0, K_0, and α_0 are obtained as the fitted parameters depending on the formulation of EoS. Previous works[18,19] adopted a Birch-Murnaghan EoS. Small K_0 in this study is due to the use of the Vinet EoS, which resulted in relatively large α_0. Thus, the difference in the value of α_0 between the present study and the previous works is not essential.

Fei *et al.*[18] evaluated the *P-V-T* EoS of ice VII from the *in situ* XRD experiments in an EHDAC at $P=6-20$ GPa and $T=300-700$ K. After 10 years, the same group[19] extended the *P-T* range of the experiment to 65 GPa and 850 K. The difference from our EoS reaches to 5.2% at $T=900$ K.[18] As mentioned above, both of the previous studies used an energy-dispersive XRD technique whose resolution is lower than the angle-dispersive technique taken in this study. Sugimura *et al.*[16] showed that the angle-dispersive XRD technique allowed one to detect the phase transitions in ice which had not been observed in the energy-dispersive techniques. In addition to the difference in XRD system, we discuss other possible sources for the discrepancies below.

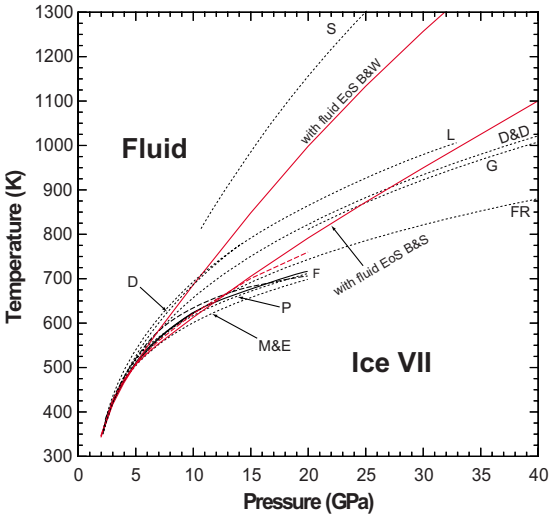

FIG. 5. (Color online) Melting curve of H_2O ice VII. The red curves are the melting lines of ice VII calculated in this study with the EoS of fluid H_2O of Brodholt and Wood (Ref. 42) (upper solid line) and Belonoshko and Saxena (Ref. 41) (lower solid line), and Halbach and Chatterjee (Ref. 40) (dashed line). The two solid red curves are taken as the upper and lower bounds in this study. The black solid and dashed lines are the result of Fei *et al.*'s (Ref. 18) calculations with the EoS of fluid H_2O from Belonoshko and Saxena (Ref. 41) and Halbach and Chatterjee (Ref. 40), respectively. The black thin dotted lines are the melting curves of ice VII proposed by previous experimental studies (Refs. 18–26) shown by letters as described in Fig. 1.

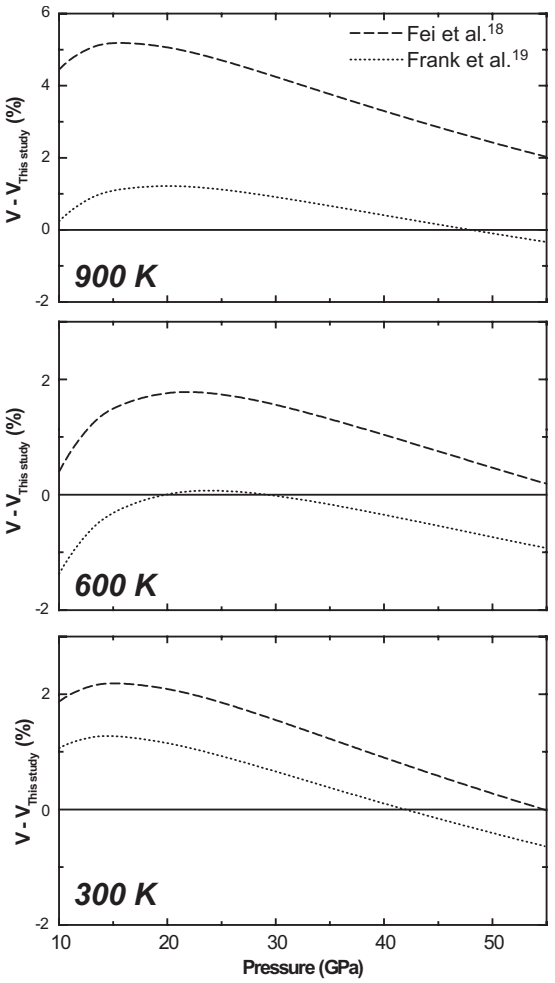

FIG. 6. Comparison of the EoS of this study (0%) with that of the previous studies (Refs. 18 and 19).

For the comparison with Fei *et al.*,[18] volumes of ice VII calculated from their EoS are larger than those calculated from our EoS by 0.0–2.2 %, 0.2–1.8 %, and 2.0–5.2 %, at $T=300$, 600, and 900 K, respectively, in the pressure range shown in Fig. 6.

In order to compare the high-P-T experimental results, attention should be paid in pressure scale.[43] Fei *et al.*[18] calculated their pressures using the Anderson *et al.*'s[44] Au scale while the present experiments determined the pressures from Fei *et al.*'s[32] Au or Pt scale. It has been pointed out[45–47] that Anderson *et al.*'s[44] Au scale underestimates the pressure compared with other Au scales, e.g., 2.4 GPa lower than Fei *et al.*'s[32] Au scale at $P=50$ GPa and $T=873$ K. However, Fig. 6 shows that the volumes of ice VII by Fei *et al.*[18] are larger than those by this study, namely, they overestimated the pressures. Thus, the discrepancy in volume of ice VII cannot be explained by the pressure scale difference.

Another possible source for the discrepancy is the nonhydrostatic environments in each experiment. In general, the nonhydrostatic condition causes an overestimation of the sample volume[48,49] as shown previously on, e.g., MgO.[33] Our P-V-T EoS of ice VII is constructed from the 300 K EoS from Sugimura *et al.*[16] and the high-temperature volume data collected in the present experiments. Sugimura *et al.*[16] evaluated the nonhydrostatic stresses on the sample via difference in lattice parameters of ice, determined separately from (110) and (200) diffraction lines. The difference does not exceed ~0.4 % even at $P=55$ GPa, which is satisfactorily small concerning the nonhydrostatic stress on the sample at $T=300$ K. For the present high-temperature experiments, the nonhydrostatic stress should be small due to the high temperature. According to Dubrovinsky *et al.*,[37] the nonhydrostatic stress can be reduced by increasing temperature and it almost vanishes at $T\geq 800$ K in a DAC at ~30 GPa. In this study, about 50% of our P-V-T data were collected at temperature well above 800 K (Table I) while Fei *et al.*'s[18] experiments were at $T\leq 650$ K, suggesting large portion of their P-V-T data were collected under highly nonhydrostatic conditions. Therefore, it is quite plausible that larger volumes of ice VII in Fei *et al.*[18] were caused by the nonhydrostatic stress on their sample.

The EoS of Frank *et al.*[19] gives volume of ice VII in better agreement with our data than Fei *et al.*[18] As in the case of Fei *et al.*,[18] the nonhydrostatic stress may account for the large volume of Frank *et al.*[19] since only about 9% of Frank *et al.*'s[19] high-temperature data set are from $T\geq 800$ K. Since all the Fei *et al.*'s[18] experiments were made at $T\leq 650$ K, the data set of Frank *et al.*'s[19] should have been taken under better hydrostatic conditions than that of Fei *et al.*[18] This is evidenced by the fact that EoS of Frank *et al.*[19] gives closer volume to ours than what Fei *et al.*'s[18] EoS gives. The hydrostaticity of the sample in our experiment is superior to the others.

At high pressures, the crossover occurs and the volumes by Frank *et al.*[19] eventually become the smallest before the pressure exceeds 48 GPa. The crossover should be accounted for the inclusion of the volume data from pressures above 40 GPa at room temperature or higher pressures at high-temperature conditions. At those high pressures, ice VII might have transformed into dynamically disordered ice VII,[16] whose volume is smaller than ice VII.

Finally, we should note a recent work by Somayazulu *et al.*[15] which proposed a ferroelastic phase transition in ice VII at $P=14$ GPa and $T=300$ K from the fact that they observed the peak broadening in XRD patterns of ice. Since present (high-T) and previous (300 K) (Ref. 16) studies did not collect the data at $P<14$ GPa, the two data set cannot directly address the change in the peak width at $P=14$ GPa, although both studies did not observe any sign of the peak broadening of ice VII at any P-T condition. Note that the peak broadening at $P=14$ GPa has never been observed in the other XRD studies as well, even with an angle-dispersive technique.[7,23,50] The peak broadening in Somayazulu *et al.*[15] could be a result of large uniaxial stress in a DAC experiment although they conducted laser annealing. The laser heating technique should have produced a large temperature gradient particularly in the compressional direction because they did not put a thermal insulator between the sample and diamond. Therefore, the stress in the sample might have been only partially released upon laser annealing. Moreover, Somayazulu *et al.*[15] used an x-ray beam with a very large diameter in order to probe the entire sample chamber so that the pressure gradient in the radial direction was also sampled. Those pressure gradients must have caused a

peak broadening. In contrast, our heating method is the external heating with a very large heater and the diameter of the x-ray beam is 15–25 % of that of the sample chamber. Our technique provides better hydrostatic environment in the probed area than Somayazulu *et al.*[15]'s.

B. Melting curve of ice VII

The melting temperature of ice VII at high pressures has been a matter of debate.[18–26] As listed above, the numbers of melting curve with different melting criteria have been proposed. Among those proposed criteria, the disappearance of XRD peaks of solid phase ice VII was criticized due to the possibility of the grain growth. Near the melting temperatures, the ice grains could rapidly grow and possibly be oriented in a direction such that the XRD appears to be absent.[22,24] Fig. 1 shows that we observed solid ice VII even in the fluid stability field in Fei *et al.*[18] and Frank *et al.*;[19] they judged melting from presence/absence of XRD peaks. Thus, Fei *et al.*[18] and Frank *et al.*[19] underestimated the stability of solid ice VII. Indeed, another melting curve[23] determined by the same XRD method is located at higher temperature than Fei *et al.*[18] and Frank *et al.*[19] These discrepancies from the same method are likely due to the grain growth of ice.

The calculated melting temperature in this study is higher than the previously calculated one[18] above $P=13$ GPa (Fig. 5), which comes from the difference in the *P-V-T* EoS for ice VII. The present experimental *P-T* conditions are within the calculated stability field of ice VII, supporting the above discussion that the *P-V-T* EoS for ice VII constructed in this study is more reliable than in Fei *et al.*[18]

The thermodynamic calculation for the melting of ice depends also on the *P-V-T* EoS for fluid H_2O. Among the numbers of proposed EoS for fluid H_2O,[40–42,51] the EoS by Belonoshko and Saxena[41] has been widely used due to its wide applicable *P-T* range (up to 100 GPa and 4000 K). Here we tested another EoS by Brodholt and Wood[42] which is also applicable in a wide *P-T* range (up to 30 GPa and 2000 K). Komabayashi *et al.*[52] argued that the fluid EoS of Brodholt and Wood[42] reproduced experimental data of a dehydration reaction of a hydrous phase up to $P=8$ GPa and $T=1100$ K and therefore, concluded this EoS was reliable. The calculated melting temperatures of ice VII differ by 300 K at $P=30$ GPa between two fluid EoS (Refs. 41 and 42) (Fig. 5). We adopted this difference as the error bar in our calculations. The melting curves by Datchi *et al.*[22] and Lin *et al.*[24] are located in this uncertainty range. The melting temperatures by Dubrovinskaia and Dubrovinsky[23] and Goncharov *et al.*[26] are somewhat lower at $P>25$ GPa but with the experimental uncertainties considered, these curves are fairly consistent with our estimates.

Figure 7 shows the densities of solid ice VII and fluid H_2O along the melting curve together with the data of Goncharov *et al.*[26] The densities of ice VII and fluid H_2O are calculated from the EoS in this study and by Belonoshko and Saxena,[41] respectively. Note that the melting temperatures of this study and Goncharov *et al.*[26] are not exactly the same and that their density data[26] are not on the equilibrium,

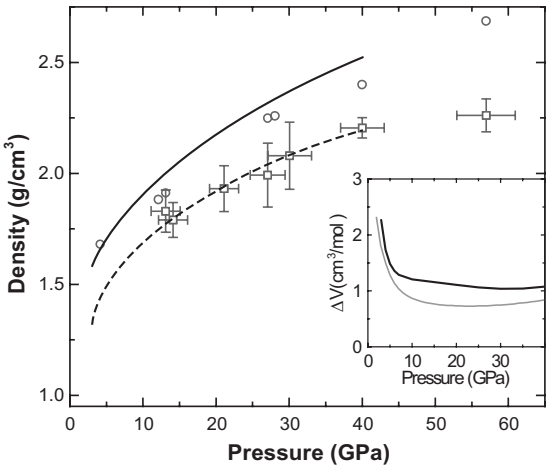

FIG. 7. Densities of ice VII and fluid H_2O along the melting curve. The densities of ice VII (black solid line) and fluid H_2O (black dashed line) are calculated from the EoS constructed in this study and from the EoS by Belonoshko and Saxena (Ref. 41), respectively. Gray symbols represents the experimental result of Goncharov *et al.* (Ref. 26): open circles, ice VII; open squares, fluid H_2O. Inset: the volume change upon melting. The black and the gray lines are of this study and of Goncharov *et al.* (Ref. 26), respectively.

namely, below and above the melting-*T* for ice VII and fluid, respectively. The density of fluid H_2O from Belonoshko and Saxena[41] is consistent with that from Goncharov *et al.*[26] as they discussed.[26] Goncharov *et al.*[26] estimated the density of fluid from the XRD data. This consistency in the volume of fluid H_2O may justify both theoretical[41] and experimental[26] estimations. In contrast, the density of solid ice VII from our EoS is larger than those from Goncharov *et al.*[26] Since Goncharov *et al.*[26] used a laser-heating technique for high-temperature runs, the uncertainty in temperature is large in their experiments. Accordingly, calculated pressures upon heating through a pressure standard may also have a large uncertainty. However, both Goncharov *et al.*[26] and this study show a similar behavior of the volume change at melting with increasing pressure (Fig. 7). Above $P=10$ GPa, the volume change is almost constant in both studies although Goncharov *et al.*[26] claimed it was slightly increased at higher pressures. This suggests that the compressibility of fluid H_2O is close to that of solid ice VII above $P=10$ GPa. Thus, the physical properties of two phases will be similar at high pressures. However, at higher pressures (at least $P>50$ GPa from this study), the dynamically disordered phases will be stabilized[16] suggesting that experimental constraints on the EoS for those high-pressure ices should be made in the near future.

The enthalpy change upon melting was calculated through thermodynamics as

$$\Delta H_m = T\Delta S_m, \tag{4}$$

where ΔH_m and ΔS_m are an enthalpy and entropy changes on melting, respectively. Figure 8 shows the calculated ΔH_m together with data from Goncharov *et al.*[26] The ΔH_m in this study is somewhat smaller (60 kJ/mol at $P=40$ GPa) than

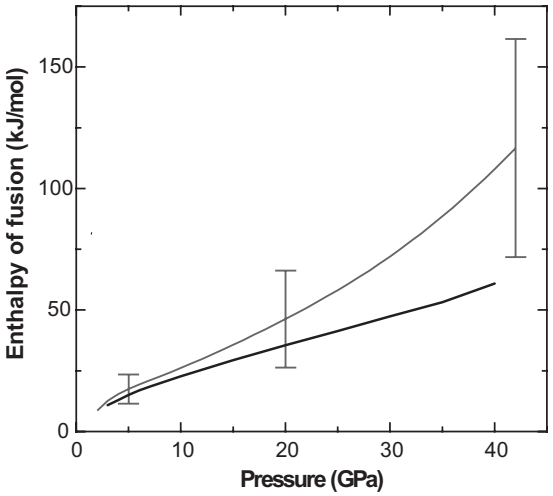

FIG. 8. Enthalpy of fusion at the melting of ice VII. Black and gray lines are of this study and of Goncharov *et al.* (Ref. 26), respectively. The error bars of Goncharov *et al.* (Ref. 26) are related to uncertainties in fluid H_2O density determination.

that of Goncharov *et al.*[26] (120 ± 45 kJ/mol) whose ΔH_m was estimated through the Clausius-Clayperon equation. Goncharov *et al.*[26] argued that such a large ΔH_m might be related to the possible dissociation reaction of fluid H_2O into H_3O^+ and OH^- at high pressures, on the basis of their first-principles calculations. However, as they discussed, their density of fluid H_2O was obtained from the XRD pattern from which the species in the fluid phase cannot be discussed. In addition, their density of fluid was well consistent with that of Belonoshko and Saxena[41] who employed a molecular-dynamics calculation assuming a H_2O molecule. Furthermore, our thermodynamic calculations were based on the fluid EoS by Belonoshko and Saxena,[41] which gave the melting line fairly consistent with that in Goncharov *et al.*[26] Therefore, the large ΔH_m in Goncharov *et al.*[26] is not likely to be the consequence of the dissociation of H_2O in the fluid. Since they derived ΔH_m through the relation of $dP/dT = \Delta H_m / T\Delta V$, the lager ΔH_m might come from the smaller ΔV, i.e., smaller density of ice VII (Fig. 7). If the density of ice VII from our EoS is used, ΔV will be larger and accordingly, ΔH_m will be smaller. Nevertheless, the possibility of the dissociation of fluid H_2O still remains as Goncharov *et al.*[26] demonstrated, independently of the ΔH_m calculations. As they discussed, if there are species of H_3O^+ and OH^- in addition to H_2O in the fluid phase, the system is no longer unary. Then, there will be a phase loop at the melting of ice, giving rise to a complex structure of the icy planets.

In conclusion, we collected volumetric data of ice VII at simultaneous high-P-T conditions with the angle-dispersive high-resolution XRD technique. The thermal EoS for ice VII was constructed in the Anderson-Grüneisen formulation. Thermodynamic calculation of the melting of ice VII shows that the melting line is located at temperatures higher than the previous calculation due to the smaller molar volume of ice VII in this study. Estimated P-T range of the melting line is consistent with the recent experimental data. The P-V-T data of ice VII and the melting curve estimated in this study provide key information for the discussions of the structure of icy planets, condensed matter physics, and material sciences.

ACKNOWLEDGMENTS

We acknowledge Y. Kuwayama, S. Tateno, R. Sinmyo, and K. Ohta for experimental and analytical help. We also thank the referees for their helpful comments. The XRD measurements were conducted at SPring-8. E.S. acknowledges support by Yoshida Scholarship Foundation and the Japan Society for the Promotion of Science for Young Scientists.

*Corresponding author; sugimura@geo.titech.ac.jp

[1] I. de Pater and J. J. Lissauer, *Planetary Sciences* (Cambridge University Press, New York, 2001).
[2] C. R. Bina and A. Navrotsky, Nature (London) **408**, 844 (2000).
[3] P. Loubeyre, R. LeToullec, E. Wolanin, M. Hanfland, and D. Hausermann, Nature (London) **397**, 503 (1999).
[4] A. Polian and M. Grimsditch, Phys. Rev. Lett. **52**, 1312 (1984).
[5] A. F. Goncharov, V. V. Struzhkin, M. S. Somayazulu, R. J. Hemley, and H. K. Mao, Science **273**, 218 (1996).
[6] K. Aoki, H. Yamawaki, M. Sakashita, and H. Fujihisa, Phys. Rev. B **54**, 15673 (1996).
[7] E. Wolanin, P. Pruzan, J. C. Chervin, B. Canny, M. Gauthier, D. Hausermann, and M. Hanfland, Phys. Rev. B **56**, 5781 (1997).
[8] M. Benoit, D. Marx, and M. Parrinello, Nature (London) **392**, 258 (1998).
[9] M. Benoit, A. H. Romero, and D. Marx, Phys. Rev. Lett. **89**, 145501 (2002).
[10] M. Benoit and D. Marx, ChemPhysChem **6**, 1738 (2005).
[11] M. Song, H. Yamawaki, H. Fujihisa, M. Sakashita, and K. Aoki, Phys. Rev. B **60**, 12644 (1999).
[12] M. Song, H. Yamawaki, H. Fujihisa, M. Sakashita, and K. Aoki, Phys. Rev. B **68**, 014106 (2003).
[13] A. F. Goncharov, N. Goldman, L. E. Fried, J. C. Crowhurst, I. Feng W. Kuo, C. J. Mundy, and J. M. Zaug, Phys. Rev. Lett. **94**, 125508 (2005).
[14] R. J. Hemley, A. P. Jephcoat, H. K. Mao, C. S. Zha, L. W. Finger, and D. E. Cox, Nature (London) **330**, 737 (1987).
[15] M. Somayazulu, J. Shu, C. S. Zha, A. F. Goncharov, O. Tschauner, H. K. Mao, and R. J. Hemley, J. Chem. Phys. **128**, 064510 (2008).
[16] E. Sugimura, T. Iitaka, K. Hirose, K. Kawamura, N. Sata, and Y. Ohishi, Phys. Rev. B **77**, 214103 (2008).
[17] M. French, T. R. Mattsson, N. Nettelmann, and R. Redmer, Phys. Rev. B **79**, 054107 (2009).
[18] Y. Fei, H. K. Mao, and R. J. Hemley, J. Chem. Phys. **99**, 5369 (1993).
[19] M. R. Frank, Y. W. Fei, and J. Z. Hu, Geochim. Cosmochim.

Acta **68**, 2781 (2004).
[20] C. W. F. T. Pistorius, M. C. Pistorius, J. P. Blakey, and L. J. Admiraal, J. Chem. Phys. **38**, 600 (1963).
[21] O. Mishima and S. Endo, J. Chem. Phys. **68**, 4417 (1978).
[22] F. Datchi, P. Loubeyre, and R. LeToullec, Phys. Rev. B **61**, 6535 (2000).
[23] N. Dubrovinskaia and L. Dubrovinsky, High Press. Res. **23**, 307 (2003).
[24] J. F. Lin, B. Militzer, V. V. Struzhkin, E. Gregoryanz, R. J. Hemley, and H. K. Mao, J. Chem. Phys. **121**, 8423 (2004).
[25] B. Schwager, L. Chudinovskikh, A. Gavriliuk, and R. Boehler, J. Phys.: Condens. Matter **16**, S1177 (2004).
[26] A. F. Goncharov, C. Sanloup, N. Goldman, J. C. Crowhurst, S. Bastea, W. M. Howard, L. E. Fried, N. Guignot, M. Mezouar, and Y. Meng, J. Chem. Phys. **130**, 124514 (2009).
[27] N. Dubrovinskaia and L. Dubrovinsky, Rev. Sci. Instrum. **74**, 3433 (2003).
[28] T. Komabayashi, K. Hirose, N. Sata, Y. Ohishi, and L. S. Dubrovinsky, Earth Planet. Sci. Lett. **260**, 564 (2007).
[29] T. Komabayashi, K. Hirose, E. Sugimura, N. Sata, Y. Ohishi, and L. S. Dubrovinsky, Earth Planet. Sci. Lett. **265**, 515 (2008).
[30] J. Hammersley, *FIT2D V12.012 Reference Manual* (European Synchrotron Radiation Facility, Grenoble, France, 1996).
[31] A. Sano, E. Ohtani, T. Kondo, N. Hirao, T. Sakai, N. Sata, Y. Ohishi, and T. Kikegawa, Geophys. Res. Lett. **35**, L03303 (2008).
[32] Y. Fei, A. Ricolleau, M. Frank, K. Mibe, G. Shen, and V. Prakapenka, Proc. Natl. Acad. Sci. U.S.A. **104**, 9182 (2007).
[33] Y. Fei, Am. Mineral. **84**, 272 (1999).
[34] S. H. Shim, T. S. Duffy, and G. Y. Shen, Phys. Earth Planet. Inter. **120**, 327 (2000).
[35] T. S. Duffy, R. J. Hemley, and H. K. Mao, Phys. Rev. Lett. **74**, 1371 (1995).
[36] S. H. Shim, T. S. Duffy, and G. Y. Shen, J. Geophys. Res. Solid Earth **105**, 25955 (2000).
[37] L. S. Dubrovinsky, S. K. Saxena, and P. Lazor, Phys. Chem. Miner. **25**, 434 (1998).
[38] O. L. Anderson, J. Geophys. Res. **72**, 3661 (1967).
[39] R. A. Robie, B. S. Hemingway, and J. R. Fisher, U. S. Geol. Surv. Bull. **1452**, 19 (1978).
[40] H. Halbach and C. D. Chatterjee, Contrib. Mineral. Petrol. **79**, 337 (1982).
[41] A. Belonoshko and S. K. Saxena, Geochim. Cosmochim. Acta **55**, 381 (1991).
[42] J. Brodholt and B. Wood, J. Geophys. Res. **98**, 519 (1993).
[43] Y. Fei, J. Li, K. Hirose, W. Minarik, J. Van Orman, C. Sanloup, W. van Westrenen, T. Komabayashi, and K. Funakoshi, Phys. Earth Planet. Inter. **143-144**, 515 (2004).
[44] O. L. Anderson, D. G. Isaak, and S. Yamamoto, J. Appl. Phys. **65**, 1534 (1989).
[45] S. H. Shim, T. S. Duffy, and K. Takemura, Earth Planet. Sci. Lett. **203**, 729 (2002).
[46] T. Katsura, H. Yamada, T. Shinmei, A. Kubo, S. Ono, M. Kanzaki, A. Yoneda, M. J. Walter, E. Ito, S. Urakawa, K. Funakoshi, and W. Utsumi, Phys. Earth Planet. Inter. **136**, 11 (2003).
[47] P. I. Dorogokupets and A. R. Oganov, Phys. Rev. B **75**, 024115 (2007).
[48] D. L. Heinz and R. Jeanloz, Phys. Rev. B **30**, 6045 (1984).
[49] Y. Sato-Sorensen, J. Geophys. Res. **88**, 3543 (1983).
[50] J. F. Lin, E. Gregoryanz, V. V. Struzhkin, M. Somayazulu, H. K. Mao, and R. J. Hemley, Geophys. Res. Lett. **32**, L11306 (2005).
[51] S. K. Saxena and Y. Fei, Geochim. Cosmochim. Acta **51**, 783 (1987).
[52] T. Komabayashi, S. Omori, and S. Maruyama, Phys. Earth Planet. Inter. **153**, 191 (2005).